Supplementary information

Neutron imaging for automotive polymer electrolyte fuel cells during rapid cold starts

Wataru Yoshimune,[*a] Yuki Higuchi,[a] Fangzhou Song,[b] Shogo Hibi,[a] Yoshihiro Matsumoto,[c] Hirotoshi Hayashida,[c] Hiroshi Nozaki,[a] Takenao Shinohara[b] and Satoru Kato[a]

[a]Toyota Central R&D Labs., Inc., Nagakute 480-1192, Japan

[b]J-PARC Center, Japan Atomic Energy Agency, Tokai 319-1195, Japan

[c]Comprehensive Research Organization for Science and Society, Tokai 319-1106, Japan

*Correspondence: yoshimune@mosk.tytlabs.co.jp

Contents
1. Detailed Setup of the Rapid Cold Start
2. Fuel Cell Degradation
3. Cooling Performance of the Cooling Unit
4. Water Storage Capacity
5. Quantitative Reliability of Water Content

1. Detailed Setup of the Rapid Cold Start

Figs. S1 and S2 show the detailed structures of the environmental chamber and the rapid heating system, respectively. An automotive polymer electrolyte fuel cell (PEFC) was placed inside the environmental chamber, and a dry gas purge was employed to prevent condensation during cooling inside the chamber. Fluorinert was circulated in the environmental chamber and on both sides of the PEFC, and a heat-exchange system was installed at the bottom of the environmental chamber. The environmental chamber was placed on a neutron-imaging stage using a crane. A commercially available chiller and an in-house rapid heating unit were placed next to the stage, and pipes were connected to pump silicone oil and ethylene glycol into the chamber. The in-house rapid heating unit constantly heated the ethylene glycol to build up the enormous amount of heat required for rapid heating, thereby assisting in the instantaneous heat requirement during a rapid cold start.
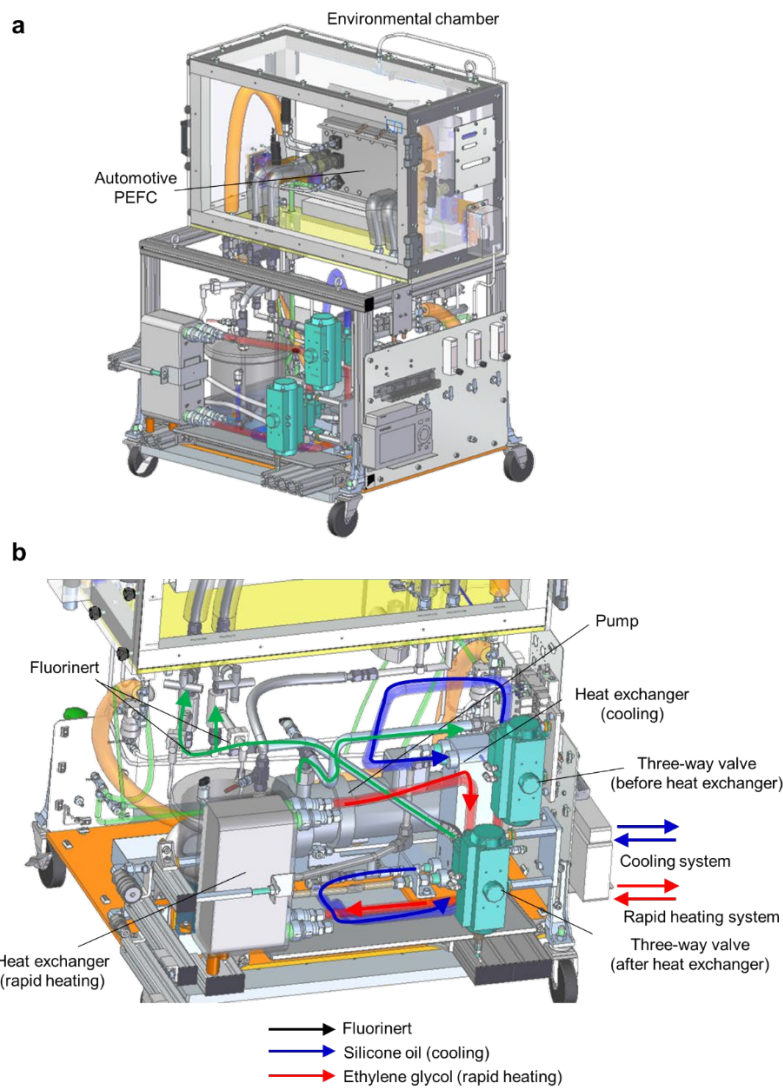

Fig. S1 Schematic representation of the environmental chamber. (a) Overview and (b) enlarged view of the environmental chamber.
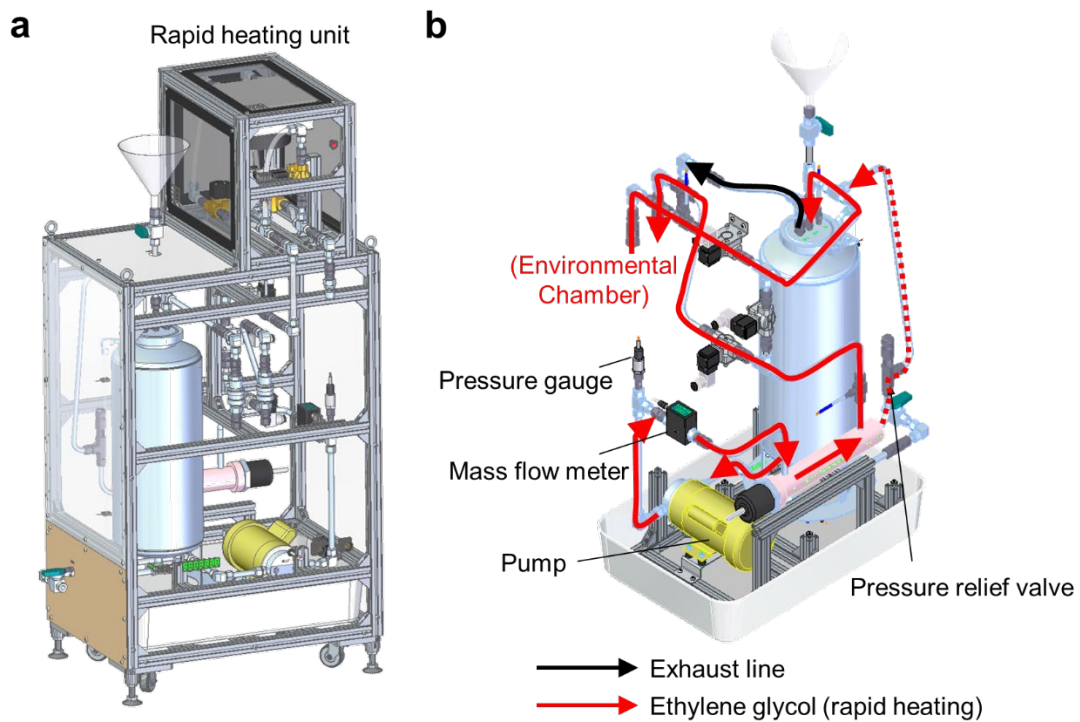
a Rapid heating unit

b

(Environmental Chamber)

Pressure gauge

Mass flow meter

Pump

Pressure relief valve

→ Exhaust line
→ Ethylene glycol (rapid heating)

Fig. S2 Schematic representation of the rapid heating unit. (a) Overview and (b) enlarged view of the rapid heating unit.

2. Fuel Cell Degradation

Fig. S3 shows that there was no significant performance degradation, even after three repeated cold-start experiments.
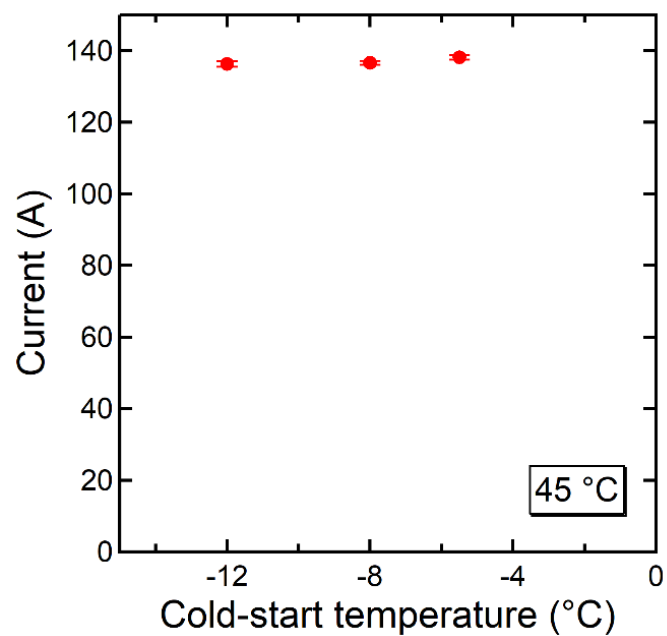

Fig. S3 Average current during power generation at 45 °C and 0.2 V for 1 min after cold-start experiments at different sub-zero temperatures.

3. Cooling Performance of the Cooling Unit

The cooling performance was evaluated by considering three directions: width (Fluorinert flow direction), height (top, centre and bottom) and depth (cathode and anode). Fig. S4 shows the cell temperature distribution during cooling to −12.0 °C. The programme start of the cold-start experiment was defined as 0 s. The cell temperature differences were Δ0.3 °C (width direction) and below Δ0.1 °C (height and depth directions).

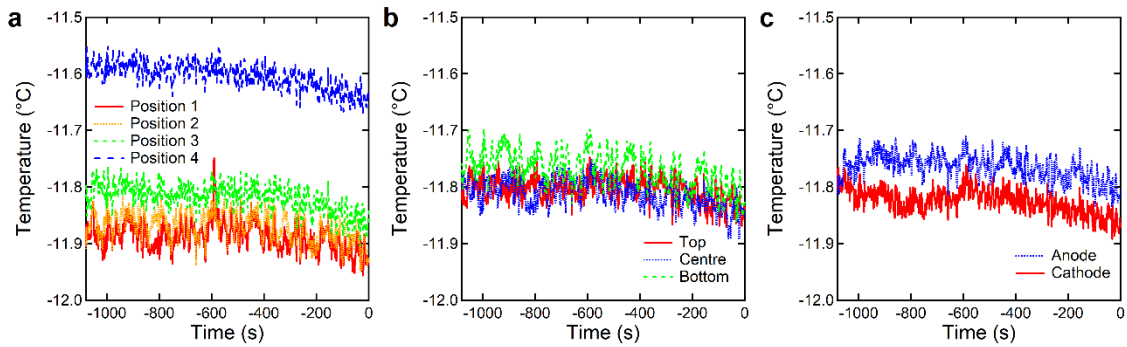**Fig. S4** Cell temperature distribution during cooling to −12.0 °C: (a) width (Fluorinert flow direction), (b) height (top, centre and bottom) and (c) depth (cathode and anode) directions.

4. Water Storage Capacity

The water storage capacity (C) of the membrane electrode assembly (MEA) can be calculated from the properties of the gas diffusion layer (GDL), the filling of the porous catalyst layer (CL) and the water uptake of the proton exchange membrane (PEM), as presented in Equation S1:

$$C = M_{\text{water}} \sum \varphi_I v_I + W_{\text{PEM}} U \qquad \text{(Equation S1)}$$

where M_{water} is the density of water, φ_I is the porosity of component I, v_I is the pore volume of component I, W_{PEM} is the weight of the PEM and U is the water uptake. The structural properties of the MEAs are summarised in Table S1 to provide a rough estimation of the water storage capacity. The reference values are based on publicly available information related to a 2nd generation MIRAI[1,2] and the results of a previous disassembly analysis.[3] With respect to the structural properties not reported as data for a 2nd generation MIRAI, representative values for typical PEFCs were used.[4–7] Fig. S5 shows the water storage capacity of each MEA component per unit geometric area. This estimation did not consider water back-diffusion to the anode. In the second water dynamics stage during the cold start, the back-diffusion effect was negligible owing to the slow rate of water diffusion in the PEM.

Table S1. Structural properties of the MEA components

MEA component	Thickness (μm)	Porosity (%)	Water uptake (wt%)
PEM	8.5[a]	—	10[g]
Cathode CL	9.1[b]	0.6–0.8[d,e]	—
Cathode GDL	240[c]	0.6–0.7[e,f]	—

[a]Ref. 1, [b]Ref. 2, [c]Ref. 3, [d]Ref. 4, [e]Ref. 5, [f]Ref. 6 and [g]Ref. 7.
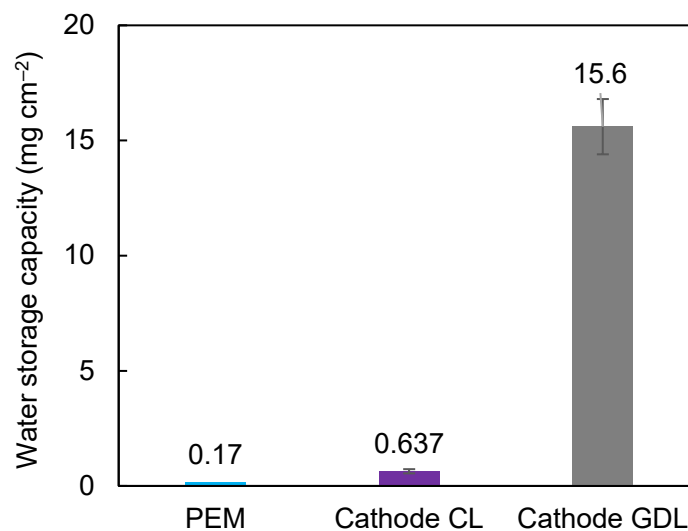

Fig. S5 Rough estimation of the water storage capacities of MEA components.

5.   Quantitative Reliability of Water Content

The water content before the cold-start experiment should be zero because the residual water inside the fuel cell was purged at the pre-conditioning step. However, the water content was scattered randomly (Fig. S6). Because the water content was obtained by dividing the dry image data with 1 s exposure by the average dry image data, it is likely affected by the intensity fluctuations of the incident neutron beams during exposure.
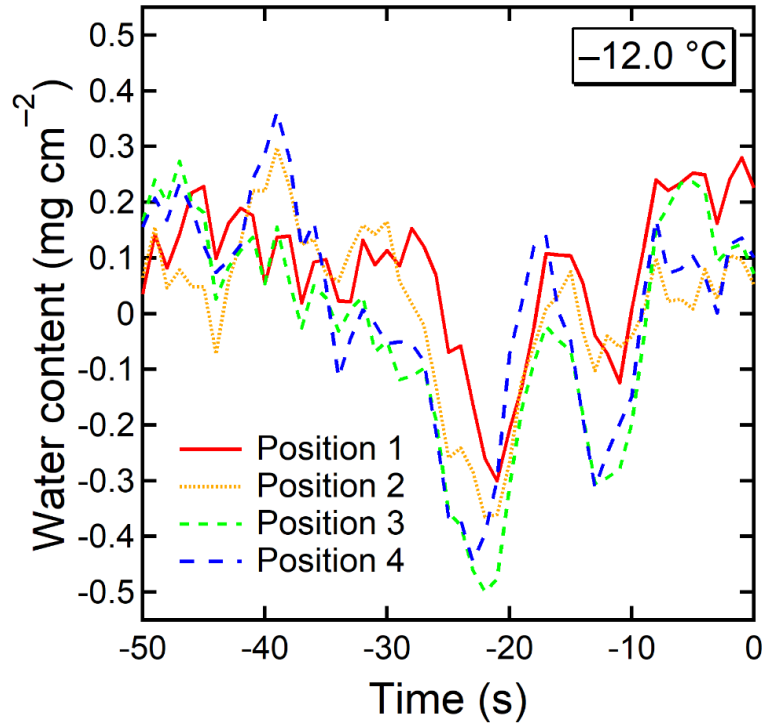

Fig. S6 Water content in the dry fuel cell before the cold-start experiment at −12.0 °C.

REFERENCES

1. W. Yoshimune, Y. Higuchi, A. Kato, S. Hibi, S. Yamaguchi, Y. Matsumoto, H. Hayashida, H. Nozaki, T. Shinohara and S. Kato, *ACS Energy Lett.*, 2023, **8**, 3485–3487.

2. New Energy and Industrial Technology Development Organization (NEDO), Fuel Cell Development Progress 2022 Report, https://www.nedo.go.jp/content/100944011.pdf, (accessed October 2024).

3. P. Von Tettau, S. Sterlepper, P. Mauermann, M. Wick, S. Tinz, M. Jesser, M. Walters and S. Pischinger, *Int. J. Hydrogen Energy*, 2024, **52**, 1127–1136.

4. Z. Yu, R. N. Carter and J. Zhang, *Fuel Cells*, 2012, **12**, 557–565.

5. S. Shukla, F. Wei, M. Mandal, J. Zhou, M. S. Saha, J. Stumper and M. Secanell, *J. Electrochem. Soc.*, 2019, **166**, F1142–F1147.

6. W. Yoshimune, S. Kato and S. Yamaguchi, *Int. J. Heat Mass Transfer*, 2020, **152**, 119537.

7. W. Yoshimune, A. Kato, T. Hayakawa, S. Yamaguchi and S. Kato, *Adv. Energy Sustainability Res.*, 2024, **5**, 2400126.